ELSEVIER

Quantum dynamics of atomic coherence in a spin-1 condensate: Mean-field versus many-body simulation

L.I. Plimak *, C. Weiß, R. Walser, W.P. Schleich

Abteilung Quantenphysik, Universität Ulm, D-89069 Ulm, Germany

Abstract

We analyse and numerically simulate the full many-body quantum dynamics of a spin-1 condensate in the single spatial mode approximation. Initially, the condensate is in a "ferromagnetic" state with all spins aligned along the y axis and the magnetic field pointing along the z axis. In the course of evolution the spinor condensate undergoes a characteristic change of symmetry, which in a real experiment could be a signature of spin-mixing many-body interactions. The results of our simulations are conveniently visualised within the picture of irreducible tensor operators.
© 2006 Elsevier B.V. All rights reserved.

1. Introduction

This paper is a tribute to Bruce Shore's role in establishing the concept of atomic coherence and the related techniques of irreducible tensor operators [1]. We demonstrate that this viewpoint emerges quite naturally when describing the evolution of a spinor condensate. During the past decade condensed Bose gases have emerged as flexible test system to explore the rich structure of many-body physics. A systematic introduction into cold gases in general and spinor condensates in particular may be found, e.g., in the book by Pethick and Smith [2]. With the development of purely optical traps [3–5], we are in the position to hold atoms with their complete hyperfine submanifold, thus entering the regime of spinor physics [2,6–9]. This is exactly the condition under which one expects the techniques of atomic coherence [1,10,11] to be most helpful.

There are two major approximations used in the literature when describing spinor condensates theoretically: the common mean-field approximation (MF) and the single mode approximation (SMA). Within the SMA, the spatial dependence of the Bose field operator describing the spinor gas is assumed given and decoupled from the internal dynamics, as illustrated schematically in Fig. 1. The reason one can separate the local redistribution of particles amongst hyperfine sublevels due to collisions from the long range dynamics is clear: a typical trapped alkali atom is paramagnetic, but provides only a single Bohr magneton of magnetic moment. Consequently the resulting magnetic dipolar interaction is very weak compared to the typical interactomic Van-der-Waals energy.

The single mode approximation is commonly introduced on top of the mean-field approximation. One exception is the paper by Koashi and Ueda [12] where the SMA is introduced directly into the many-body treatment (see also [2]). This, and also neglecting the quadratic Zeeman part of the energy, allowed the authors to construct an explicit solution to the problem including collisions. In this paper we include the quadratic Zeeman part which plays a crucial role in the dynamics of the condensate as realized with ^{87}Rb or ^{23}Na atoms [5,13,14]. Consequently, we are

---

* Corresponding author.
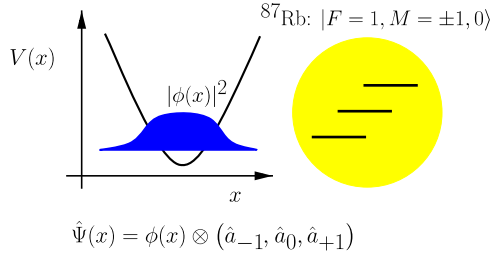*E-mail address:* lev.plimak@uni-ulm.de (L.I. Plimak).

Fig. 1. Schematic diagram of the harmonically trapped spin-1 ^{87}Rb condensate in the single-mode approximation.

left with an interacting three mode Hamiltonian, whose dynamics will be the subject of study in this article.

It should be pointed out that our approach would not apply directly to the recently realised Chromium Bose–Einstein condensate [15] where the dipolar interaction is comparable to the Van-der-Waals energy. Even less so in the case of heteronuclear molecules pursued by many experimental groups around the world where the dipolar interaction is expected to be the dominant mechanism. Independence of the internal and spatial motion is completely lifted e.g. in the proposed Einstein–de Haas effect [16,17]. The SMA is obviously not applicable under the conditions for condensate fragmentation and domain formation (see [18] and references therein).

The article is organized as follows: In Section 2 we review the derivation of the three mode spinor Hamiltonian. For later reference, we will also discuss the standard mean-field approximation in the language of Hamiltonian mechanics in Section 3. Visualizing the results of a full many-body evolution of the three mode system is a nontrivial problem. Therefore, we introduce the concepts of irreducible tensor operators in Section 4. Finally, we discuss and compare the results of the many-body calculation in Section 5.

2. Many-body approach to spinor condensate dynamics

The $F = 1$ bosons are described in the usual way by a field operator with the three spherical components, $\hat{\psi}_k(\mathbf{r})$, where $k = 1, 0, -1$ (in this order) labels the z projection of the atomic spin. The effective low energy Hamiltonian of such bosons in a homogeneous magnetic field is written as: (cf. [5,6,13,19])

$$\hat{\mathscr{H}} = \hat{\mathscr{H}}_0 + \hat{\mathscr{H}}_B + \hat{\mathscr{H}}_{\text{coll}}^{(0)} + \hat{\mathscr{H}}_{\text{coll}}^{(2)}. \tag{1}$$

Here,

$$\hat{\mathscr{H}}_0 = \sum_k \int d^3\mathbf{r}\, \hat{\psi}_k^\dagger(\mathbf{r}) \left[-\frac{\hbar^2}{2M}\Delta + U(\mathbf{r}) \right] \hat{\psi}_k(\mathbf{r}), \tag{2}$$

contains the kinetic energy and the trapping potential which holds the atoms in place, and

$$\hat{\mathscr{H}}_B = \sum_k E_k \int d^3\mathbf{r}\, \hat{\psi}_k^\dagger(\mathbf{r}) \hat{\psi}_k(\mathbf{r}) = \sum_k E_k \hat{\mathscr{N}}_k, \tag{3}$$

describes the effects of the magnetic field. For weaker magnetic fields, this is mainly the linear Zeeman effect,

$E_1 - E_0 \approx E_0 - E_{-1} \propto B$, and the quadratic Zeeman, or Paschen–Back effect, $E_1 + E_{-1} - 2E_0 \propto B^2$. The latter is crucial for the purposes of our analyses. The general Breit–Rabi formulas for E_k may be found in Ref. [20].

Both $\hat{\mathscr{H}}_0$ and $\hat{\mathscr{H}}_B$ describe single-body physics. Two-body collisions enter via $\hat{\mathscr{H}}_{\text{coll}}^{(0)}$ and $\hat{\mathscr{H}}_{\text{coll}}^{(2)}$. The former describes the familiar spin-independent density–density interaction,

$$\hat{\mathscr{H}}_{\text{coll}}^{(0)} = \frac{c_0}{2} \sum_{k,l} \int d^3\mathbf{r}\, \hat{\psi}_k^\dagger(\mathbf{r})\hat{\psi}_l^\dagger(\mathbf{r})\hat{\psi}_l(\mathbf{r})\hat{\psi}_k(\mathbf{r}) = \frac{c_0}{2} \int d^3\mathbf{r} : \hat{n}^2(\mathbf{r}) :, \tag{4}$$

where $\hat{n}(\mathbf{r}) = \sum_k \hat{n}_k(\mathbf{r}) = \sum_k \hat{\psi}_k^\dagger(\mathbf{r})\hat{\psi}_k(\mathbf{r})$, and $: :$ stands for the normal ordering of the field operators. The latter describes the spin-dependent part of the collision,

$$\hat{\mathscr{H}}_{\text{coll}}^{(2)} = \frac{c_2}{2} \int d^3\mathbf{r} : \hat{\mathscr{F}}^2(\mathbf{r}) :, \tag{5}$$

where $\hat{\mathscr{F}}(\mathbf{r})$ is the density of the angular momentum of the condensate,

$$\hat{\mathscr{F}}_s(\mathbf{r}) = \sum_{k,l} [F_s]_{kl} \hat{\psi}_k^\dagger(\mathbf{r})\hat{\psi}_l(\mathbf{r}). \tag{6}$$

The Cartesian components of the single-particle spin operator, $\mathbf{F}$, are defined as: [11]

$$F_x = \frac{1}{\sqrt{2}}\begin{pmatrix} 0 & 1 & 0 \\ 1 & 0 & 1 \\ 0 & 1 & 0 \end{pmatrix}, \quad F_y = \frac{i}{\sqrt{2}}\begin{pmatrix} 0 & -1 & 0 \\ 1 & 0 & -1 \\ 0 & 1 & 0 \end{pmatrix},$$

$$F_z = \begin{pmatrix} 1 & 0 & 0 \\ 0 & 0 & 0 \\ 0 & 0 & -1 \end{pmatrix}. \tag{7}$$

The collisional interaction constants, c_0 and c_2, are expressed in terms of the scattering lengths a_0 and a_2, for two spin-1 atoms in the combined symmetric channels of total spins, respectively, 0 and 2, as [6]

$$c_0 = \frac{4\pi\hbar^2(a_0 + 2a_2)}{3M}, \quad c_2 = \frac{4\pi\hbar^2(a_2 - a_0)}{3M}. \tag{8}$$

A typical value of c_2 is one-two orders of magnitude below c_0. This leads to a natural separation of time scales: on smaller time scales, one may neglect $\hat{\mathscr{H}}_{\text{coll}}^{(2)}$, whereas for longer time scales it may be of crucial importance. The ultimate example of a longer time scale is the ground state of the condensate, which may be polar or ferromagnetic depending on the sign of c_2 [6]. An example of the opposite are experiments where the spinor condensate is prepared in a particular magnetic state, and the evolution of the condensate is then observed [5,13,21]. In this case, an approximation commonly used in the literature is the so-called single mode approximation (SMA). Technically, SMA is recovered by assuming that the spatial dependence of the field operator is fixed, $\hat{\psi}_k(\mathbf{r}) = \phi(\mathbf{r})\hat{a}_k$, $\int d^3\mathbf{r}|\phi(\mathbf{r})|^2 = 1$. Under the SMA, the Hamiltonian of the system of N spin-one particles becomes: (cf. [12])

$$\hat{\mathscr{H}} = -p\widehat{F_z} + q\widehat{F_z^2} + \frac{g_2}{2} : \hat{\mathscr{F}}^2 :$$
$$= -p\hat{\mathscr{F}}_z + q\widehat{F_z^2} + \frac{g_2}{2}(\hat{\mathscr{F}}^2 - 2\hat{\mathscr{N}}). \tag{9}$$

Here, $g_2 = c_2 \int d^3\mathbf{r}|\phi(\mathbf{r})|^4$, $p = (E_{-1} - E_1)/2$, and $q = (E_1 + E_{-1})/2 - E_0$. The "wide hat" symbol denotes mapping of a single-body operator into the Fock space,

$$\widehat{A} = \sum_{k,l} \hat{a}_k^\dagger A_{kl}\hat{a}_l, \tag{10}$$

with $\hat{a}_l$ being the mode annihilation operators; in our case, $l = 1, 0, -1$ (in this order). The "wide hat" should not be confused with the "normal" hat which just signifies that a quantity is an operator in the Fock space. In particular, $\hat{\mathscr{F}} = \widehat{\mathbf{F}}$ is the full angular momentum operator, and $\hat{\mathscr{N}} = \widehat{\mathscr{I}_3}$ is the Fock-space operators of the total particle number, where $\mathscr{I}_3$ is a 3×3 unit matrix. The second line in Eq. (9) is found using that,

$$: \hat{\mathscr{F}}^2 := \hat{\mathscr{F}}^2 - \widehat{\mathbf{F}^2} = \hat{\mathscr{F}}^2 - 2\hat{\mathscr{N}}. \tag{11}$$

In numerical terms, constituents of Eq. (9) are sparse matrices; these are handled very efficiently by common high-level numerical packages. Some details on how these were implemented numerically may be found in Appendix A.

3. The canonical formulation of the mean-field dynamics

3.1. Introducing the mean field

In the mean field approximation, operators $\hat{a}_k$ are replaced by complex numbers ζ_k. However, this transition is not uniquely defined. Using different orderings (normal, symmetric, etc.) of creation and annihilation operator yields different *functional forms* of the quantum Hamiltonian. In quantum mechanics these functional forms represent the same Hamiltonian. In the mean field picture where ordering is immaterial for the complex numbers ζ_k, ζ_k^*, these different functional forms result in different classical Hamiltonians. In the scalar case, the corresponding corrections are of the order of $1/N$, where N is the total number of atoms. For the spinor condensate, these corrections are of the order of one over the population of Zeeman sublevels. There can well be pathological cases when one level is much depleted, leading to large corrections. It is therefore of importance to have the procedure of introducing the mean field approximation for the spinor condensate clearly defined.

There is a number of ways the mean field picture can be introduced. The most rigorous one is via the phase-space technique (see, e.g., [22] and references therein), where the time-dependent Gross–Pitaevskii equation appears on dropping quantum noises in the equations for the phase-space amplitudes. This procedure is equivalent to using the normally ordered form of the interaction Hamiltonian, replacing the field operators by the c-numbers, and then *postulating* the resulting c-number function to be the classical Hamiltonian. The lack of rigour is clearly seen in the fact that this procedure leaves it unclear how quantum averages are expressed by the c-number amplitudes. Some insight can be gained from the fact that if we postulate the many body state as a coherent state, $|\zeta\rangle = |\zeta_1\rangle|\zeta_0\rangle|\zeta_{-1}\rangle$, and then minimize the energy subject to the condition $\langle\zeta|\hat{\mathscr{N}}|\zeta\rangle = \|\zeta\|^2 = N$, the time-independent Gross–Pitaevskii equation is recovered. This recipe is in fact general: a correct mean-field expression for the average of an operator $\hat{\mathscr{X}}$ is found as $\langle\hat{\mathscr{X}}\rangle = \langle\zeta|\hat{\mathscr{X}}|\zeta\rangle$. This is equivalent to replacing field operators by c-numbers in the *normally ordered representation* of $\hat{\mathscr{X}}$.

3.2. The classical Hamilton equations of motion

Following the above recipe, we postulate the classical Hamilton function to be,

$$H(\zeta, \pi) = \langle\zeta|\hat{\mathscr{H}}|\zeta\rangle$$
$$= -p(|\zeta_1|^2 - |\zeta_{-1}|^2) + q(|\zeta_1|^2 + |\zeta_{-1}|^2) + \frac{g_2}{2}[|\zeta_1|^4$$
$$+ |\zeta_{-1}|^4 - 2|\zeta_1|^2|\zeta_{-1}|^2 + 2|\zeta_0|^2|\zeta_1|^2 + 2|\zeta_0|^2|\zeta_{-1}|^2$$
$$+ 2\zeta_0^2\zeta_1^*\zeta_{-1}^* + 2\zeta_0^{*2}\zeta_1\zeta_{-1}], \tag{12}$$

where Eq. (9) was used to find the explicit form of the Hamilton function. To use the powerful methods of analytical mechanics we have to know the canonical conjugated momentum π to the coordinate ζ. If, by definition, $\mathbf{x}$ and $\mathbf{p}$ are three-dimensional canonical conjugated variables, defining the complex variable ζ

$$\zeta = \frac{\mathbf{x} + i\mathbf{p}}{\sqrt{2}}, \tag{13}$$

than we can identify $\pi = i\zeta^*$. One can verify easily, that this is a proper canonical transform, as

$$\{\zeta_i, \pi_l\}_{\{x,p\}} = \delta_{il}, \tag{14}$$

with the following conventional definition of the Poisson brackets,

$$\{F, G\}_{\{x,p\}} = \sum_{i=\pm1,0} \frac{\partial F}{\partial x_i}\frac{\partial G}{\partial p_i} - \frac{\partial F}{\partial p_i}\frac{\partial G}{\partial x_i}. \tag{15}$$

So we obtain the Hamilton equations of motion

$$\frac{d}{dt}\zeta_l = \{\zeta_l, H(\zeta, \pi)\}_{\{\zeta,\pi\}} = \frac{\partial H(\zeta, \pi)}{\partial\pi_l},$$
$$\frac{d}{dt}\pi_l = \{\pi_l, H(\zeta, \pi)\}_{\{\zeta,\pi\}} = -\frac{\partial H(\zeta, \pi)}{\partial\zeta_l}. \tag{16}$$

By employing complex coordinates we have doubled the dimension of the phase space making the two sets of equations of motion redundant. Explicitly, we find the three components of the time-dependent Gross–Pitaevskii equation

$$i\frac{d}{dt}\zeta = (H_0 + g_2H_1)\zeta, \tag{17}$$

$$H_0 = \begin{bmatrix} -p+q & 0 & 0 \\ 0 & 0 & 0 \\ 0 & 0 & p+q \end{bmatrix},$$

$$H_1 = \begin{bmatrix} |\zeta_0|^2 + \mathscr{F}_z & \zeta_{-1}^*\zeta_0 & 0 \\ \zeta_{-1}\zeta_0^* & |\zeta_1|^2 + |\zeta_{-1}|^2 & \zeta_1\zeta_0^* \\ 0 & \zeta_1^*\zeta_0 & |\zeta_0|^2 - \mathscr{F}_z \end{bmatrix}, \qquad (18)$$

with $\mathscr{F}_z = |\zeta_1|^2 - |\zeta_{-1}|^2$. For the initial condition as in the experiment of the Sengstock group [5], these nonlinear equations have been solved analytically in terms of the periodic Jacobi elliptic functions, see [14].

3.3. Comparing the many-body and mean-field dynamics

Consider now how an effective mean-field amplitude is recovered in the many-body techniques. Were the population and coherence properties of the matter field investigated in a measurement, all the relevant information enters through the single-body density matrix,

$$\rho_{lk}(t) = \langle \Psi_0 | \hat{a}_k^\dagger(t)\hat{a}_l(t) | \Psi_0 \rangle, \qquad (19)$$

where $|\Psi_0\rangle$ is the initial many-body state, and $\hat{a}_l(t)$ is the Heisenberg field operator,

$$\hat{a}_l(t) = \hat{\mathscr{U}}(t)^\dagger \hat{a}_l \hat{\mathscr{U}}(t), \quad \hat{\mathscr{U}}(t) = \exp(-i\hat{\mathscr{H}}t). \qquad (20)$$

It can be also written as an object in the Schrödinger picture,

$$\rho_{lk}(t) = \langle \Psi_0(t) | \hat{a}_k^\dagger \hat{a}_l | \Psi_0(t) \rangle, \qquad (21)$$

where $|\Psi_0(t)\rangle = \hat{\mathscr{U}}(t)|\Psi_0\rangle$. The order or matrix indices was chosen so as to have a natural property,

$$\langle \Psi_0(t) | \widehat{A} | \Psi_0(t) \rangle = \mathrm{Tr}\rho(t)A, \qquad (22)$$

for any single-body operator A. The "wide hat" symbol is defined by Eq. (10). In the mean-field approach, the density matrix is expressed by the mean-field amplitude, $\zeta(t)$, as:

$$\rho_{lk}^{\mathrm{MF}}(t) = \zeta_l(t)\zeta_k^*(t). \qquad (23)$$

Mathematically speaking, this relation stipulates that ρ^{MF} has a single nonzero eigenvalue equal to N, with $N^{-1/2}\zeta(t)$ being the corresponding eigenvector. It is then only natural to introduce effective mean-field amplitudes as eigenvectors of $\rho(t)$:

$$\rho_{lk}(t) = \sum_{s=1,2,3} r_s(t)\zeta_l^{(s)}(t)\zeta_k^{(s)*}(t), \quad \zeta^{(s)} \cdot \zeta^{(s')*} = N\delta_{ss'}. \qquad (24)$$

In general, we have three eigenvectors of $\rho(t)$, $N^{-1/2}\zeta^{(s)}(t)$, and three related eigenvalues, $Nr_s(t)$, $r_1(t) + r_2(t) + r_3(t) = 1$. For a mean-field approximation to be recovered, there must exist a dominant eigenvalue, $r_1(t) \gg r_2(t), r_3(t)$. Below in Section 5 we shall see that it is exactly the situation occurring at early stages of the condensate evolution. At later stages all three eigenvalues are of the same order of magnitude so that the mean-field approximation breaks down completely.

4. Time evolution of atomic coherence

4.1. Irreducible tensor operators

The physical information contained in the correlations expressed by the single-body density matrix is *atomic coherence* [1]. A natural framework for discussing such correlations is the picture of irreducible tensor operators [1,10,11]. An irreducible tensor operator of angular momentum j is a set of $2j+1$ square matrices, T_{jm}, $m = -j, -j+1, \ldots, j$. Under three dimensional rotations, they obey the same transformation laws as spherical harmonics $Y_{jm}(\theta, \phi)$, thus forming a natural basis for expressing any physical quantity with angular momentum j. Furthermore, irreducible tensor operators form a full orthonormal set in the space of matrices in respect of the Hilbert–Schmidt norm:

$$\mathrm{Tr} T_{jm} T_{j'm'}^\dagger = \delta_{jj'}\delta_{mm'}, \qquad (25)$$

and for any $(2J+1) \times (2J+1)$ matrix A,

$$A = \sum_{j=0}^{2J} \sum_{m=-j}^{j} c_j^m T_{jm}, \quad c_j^m = \mathrm{Tr} T_{jm}^\dagger A. \qquad (26)$$

4.2. Dipole and quadrupole momenta of the spin-1 condensate

4.2.1. Cyclic basis

For the spin-1 condensate, the single-body density matrix equation (19) is a 3×3 matrix and hence only contains angular momenta 0, 1, and 2:

$$\rho(t) = c_0^0 T_{00} + \sum_{m=-1}^{1} c_1^m T_{1m} + \sum_{m=-2}^{2} c_2^m T_{2m}. \qquad (27)$$

c_0^0 and c_1^m have a very simple interpretation: c_0^0 is in essence the total population,

$$c_0^0 = \frac{1}{\sqrt{3}} \langle \hat{\mathscr{N}} \rangle = \frac{N}{\sqrt{3}}, \qquad (28)$$

and c_1^m is related to magnetisation,

$$c_1^m = -\frac{1}{\sqrt{2}} \langle \hat{\mathscr{F}}_m \rangle^*, \qquad (29)$$

where the spherical components of the angular momentum operator are defined as, $\hat{\mathscr{F}}_\pm = \mp(\hat{\mathscr{F}}_x \pm i\hat{\mathscr{F}}_y)/\sqrt{2}$, $\hat{\mathscr{F}}_0 = \hat{\mathscr{F}}_z$. $c_{2\mu}$ characterise the quadrupole momentum (alignment) of the atomic state.

4.2.2. Cartesian basis

It is instructive to rewrite $\rho(t)$ in the Cartesian basis, (with $\alpha, \beta = x, y, z$)

$$\rho_{\alpha\beta}(t) = \langle \Psi_0 | \hat{a}_\beta^\dagger(t)\hat{a}_\alpha(t) | \Psi_0 \rangle,$$
$$\hat{a}_\pm = \mp(\hat{a}_x \pm i\hat{a}_y)/\sqrt{2}, \quad \hat{a}_0 = \hat{a}_z. \qquad (30)$$

Then, atomic population corresponds to the trace of the density matrix, magnetisation – to its antisymmetric part, and alignment – to its traceless symmetric part. Taking the

symmetric part of an Hermitian matrix is the same as taking its real part, hence $\Re\rho$ contains a mix of the population and alignment while $\Im\rho$ is pure magnetisation. Explicitly,

$$\rho_{\alpha\beta} = \Re\rho_{\alpha\beta} + \Im\rho_{\alpha\beta} = \Re\rho_{\alpha\beta} + \frac{i}{2}\sum_\sigma \varepsilon_{\alpha\beta\sigma}\mathscr{F}_\sigma,$$

$$\mathscr{F}_\sigma = -i\sum_{\alpha,\beta}\varepsilon_{\alpha\beta\sigma}\rho_{\alpha\beta}, \tag{31}$$

where $\mathscr{F} = \langle\hat{\mathscr{F}}\rangle$ is the magnetisation vector, and $\varepsilon_{\alpha\beta\sigma}$ is the fully antisymmetric tensor, $\varepsilon_{\alpha\beta\sigma} = -\varepsilon_{\beta\alpha\sigma} = -\varepsilon_{\alpha\sigma\beta}$, $\varepsilon_{xyz} = 1$. Introducing the quadrupole tensor as per Ref. [11],

$$Q_{\alpha\beta} = \frac{N}{3}\delta_{\alpha\beta} - \Re\rho_{\alpha\beta}, \tag{32}$$

we find the irreducible-tensor-operator expansion of $\rho(t)$ as

$$\rho_{\alpha\beta} = \frac{N}{3}\delta_{\alpha\beta} + \frac{i}{2}\sum_\sigma \varepsilon_{\alpha\beta\sigma}\mathscr{F}_\sigma - Q_{\alpha\beta}. \tag{33}$$

4.3. Atomic coherence under the mean-field approximation

In the mean-field picture, $\rho_{\alpha\beta} = \zeta_\alpha\zeta_\beta^*$, where the Cartesian components of $\zeta = \zeta' + i\zeta''$ are found in full analogy to Eq. (30). The population-and-alignment part of the density matrix is then,

$$\Re\rho_{\alpha\beta} = \zeta'_\alpha\zeta'_\beta + \zeta''_\alpha\zeta''_\beta. \tag{34}$$

Magnetisation also follows easily,

$$\mathscr{F} = -2[\zeta' \times \zeta'']. \tag{35}$$

We can assume that either ζ is real, $\zeta'' = 0$, or the real and imaginary parts of ζ are orthogonal, $\zeta' \perp \zeta''$. Indeed, since we can always find such φ that

$$\Re\zeta e^{i\varphi} \cdot \Im\zeta e^{i\varphi} = \zeta' \cdot \zeta'' \cos 2\varphi + \frac{\zeta'^2 - \zeta''^2}{2}\sin 2\varphi = 0, \tag{36}$$

this orthogonality can be achieved by an overall phase transformation. Then, Eq. (34) explicitly diagonalises $\Re\rho$, making it evident that in the mean-field approximation $\Re\rho$ always has a zero eigenvalue. Another two eigenvalues equal ζ'^2 and ζ''^2. If ζ is real, two eigenvalues of $\Re\rho$ are zeros, leaving the system in a maximal-alignment state along ζ. In this case, the magnetisation which is related to $\Im\rho$ vanishes. The inverse is also true: zero magnetisation is characteristic of real ζ.

An immediate word of caution is necessary here. Orthogonality of $\Re\zeta$ and $\Im\zeta$ is not preserved by the Gross–Pitaevskii equation (17). One can rewrite Eq. (17) so as to maintain the said orthogonality, but the resulting equations are rather bulky and do not seem to allow for a new insight; worse still, under certain conditions the phase evolution is discontinuous.

4.4. Equations of motion for the atomic coherence

In order to gain further insight into the evolution of the atomic coherence, consider the equations of motion for the single-body density matrix written in terms of the magnetisation and quadrupole matrix. Direct calculation with Hamiltonian equation (9) yields,

$$\dot{\mathscr{F}}_\alpha = \sum_\sigma \varepsilon_{\alpha\sigma z}(p\mathscr{F}_\sigma + 2qQ_{\sigma z}),$$

$$\dot{Q}_{\alpha\beta} = \sum_\sigma \varepsilon_{\alpha\sigma z}\left(pQ_{\sigma\beta} + \frac{q}{2}\delta_{\beta z}\mathscr{F}_\sigma\right) + \{\alpha \leftrightarrow \beta\} + [\dot{Q}_{\alpha\beta}]_{\text{coll.}} \tag{37}$$

The benefits of the representation of irreducible tensor operators are now clearly seen. Collisions are spherically symmetric so that only the linear and quadratic Zeeman effects may couple magnetisation and alignment. In actuality, additional reflection symmetries leave only quadratic Zeeman effect to do it. The linear Zeeman effect leads only to the overall Larmor precession around the z axis. Furthermore, collisions only contribute directly to the evolution of the quadrupole,

$$[\dot{Q}_{\alpha\beta}]_{\text{coll.}} = 2g_2\Im\sum_\sigma\langle\hat{a}_\alpha^\dagger\hat{a}_\beta^\dagger\hat{a}_\sigma^2\rangle. \tag{38}$$

In general, this contribution contains nontrivial two-body correlations and cannot be simplified any further. Within the mean-field approximation,

$$[\dot{Q}_{\alpha\beta}]_{\text{coll.}} = 2g_2[2(\zeta' \cdot \zeta'')(\zeta'_\alpha\zeta'_\beta - \zeta''_\alpha\zeta''_\beta) - (\zeta'^2 - \zeta''^2)(\zeta'_\alpha\zeta''_\beta + \zeta''_\alpha\zeta'_\beta)]. \tag{39}$$

Note that here we do not assume that $\zeta' \perp \zeta''$.

Eq. (37) allow one to make qualitative statements about the evolution of the system's coherence independently of the details of collisional interactions. Assume that the initial state of the system is as in experiment [5]. Then, the initial magnetization vector is along the x axis, $\mathscr{F}_z = 0$. Since $\dot{\mathscr{F}}_z = 0$, cf. Eq. (37), magnetization $\mathscr{F}$ never leaves the xy plane. As a result, under the mean field approximation the alignment eigenvectors stay in a plane orthogonal to the xy plane, cf. Eq. (35). If at a particular time magnetisation vanishes, the mean field picture predicts that the system must be axially symmetric. Hence, under the SMA, absence of axial symmetry at zero magnetisation is a clear signature of many-body effects. Since thermalisation via symmetric collisions can only increase the symmetry of the system, it appears plausible that this statement should survive beyond the SMA. Verifying this conjecture is subject to further analysis.

5. Results and discussion

5.1. Fock space of the spinor condensate

The choice of the basis in the Fock space is inherently linked to the angular-momentum properties of Hamiltonian Eq. (9). A native bookkeeping is to introduce the basis states by the populations of the single-particle states with $F_z = 1, 0, -1$. By construction, such basis state in the Fock space is an eigenstate of the three mode population operators:

$$\hat{\mathscr{N}}_k|N_1, N_0, N_{-1}\rangle = N_k|N_1, N_0, N_{-1}\rangle, \quad k = 1, 0, -1. \quad (40)$$

These states also happen to be the eigenstates of $\hat{\mathscr{N}}$ and $\hat{\mathscr{F}}_z$:

$$\hat{\mathscr{N}}|N_1, N_0, N_{-1}\rangle = N|N_1, N_0, N_{-1}\rangle,$$
$$\hat{\mathscr{F}}_z|N_1, N_0, N_{-1}\rangle = M|N_1, N_0, N_{-1}\rangle, \quad (41)$$

where $N = N_1 + N_0 + N_{-1}$ and $M = N_1 - N_{-1}$. Since $\hat{\mathscr{H}}$ commutes with $\hat{\mathscr{N}}$ and $\hat{\mathscr{F}}_z$, states with different N's and M's are not mixed by free evolution. Another simplification when using this "natural" basis is the ease with which the many-body operators are implemented (Appendix A).

In the absence of the quadratic Zeeman effect (QZE), Hamiltonian equation (9) conserves the full angular momentum, $\hat{\mathscr{F}}^2$, and its component, $\hat{\mathscr{F}}_z$. In this case the time evolution is solved [12] by simply classifying the basis states by the eigenvalues of the three operators:

$$\hat{\mathscr{N}}|N, F, M\rangle_{\mathscr{F}} = N|N, F, M\rangle_{\mathscr{F}},$$
$$\hat{\mathscr{F}}^2|N, F, M\rangle_{\mathscr{F}} = F(F + 1)|N, F, M\rangle_{\mathscr{F}}, \quad (42)$$
$$\hat{\mathscr{F}}_z|N, F, M\rangle_{\mathscr{F}} = M|N, F, M\rangle_{\mathscr{F}}.$$

Here, $0 \leqslant F \leqslant N$ and $-F \leqslant M \leqslant F$. The subscript $\mathscr{F}$ distinguishes the "angular momentum" basis from the "natural" basis introduced above.

In the presence of the QZE, F is not a good quantum number any more, while M is still conserved. Hamiltonian Eq. (9) can then be diagonalised within subspaces of given M of the "natural" basis. Conversely, rotating the states by the radio-frequency field as in Ref. [5] conserves F while mixing different M's. Using the "angular momentum" basis may thus be of some help. In the calculations summarised in this paper, the natural basis was used. Exploring the advantages of the angular momentum basis remains a subject to further work.

5.2. Numerical procedure and the choice of parameters

All simulations summarised in this paper were carried out with the experiment by Sengstock and co-workers in mind [5]. In this experiment, the condensate is firstly prepared in a state where all atomic spins are antiparallel to the z axis. A radio-frequency pulse is then used to re-orient the spins antiparallel to the x axis. In our notation, this state looks as

$$|\Psi_0\rangle = \exp(-\mathrm{i}\vartheta\hat{\mathscr{F}}_y)|0, 0, N\rangle, \quad (43)$$

where $\vartheta = \pi/2$. Since the manifold of $M = -N$ is non-degenerate, $|0, 0, N\rangle$ is also an eigenstate of the total angular momentum, $|0, 0, N\rangle = |N, N, -N\rangle_{\mathscr{F}}$. Furthermore, since the evolution does not mix different M's, $|0, 0, N\rangle$ must be an eigenstate of the Hamiltonian, providing us with a test of numerics. Another test is setting $\vartheta = \pi$, yielding $|\Psi_0\rangle = |N, 0, 0\rangle = |N, N, N\rangle_{\mathscr{F}}$, which is also an eigenstate of the Hamiltonian. Having thus checked that both for $\vartheta = 0$ and for $\vartheta = \pi$ "nothing at all happens," we proceeded with a series of simulations with $\vartheta = \pi/2$.

To compare the many-body results to the mean-field approximation, we also ran a mean-field simulation of the system using Eq. (17). It easy to see that, with our choice of the many-body initial state, Eqs. (23) are exact at $t = 0$. This provides us with the initial condition for the mean-field simulation. This is certainly the same initial mean-field amplitude as used in Refs. [5,14].

Simulations presented in this paper were run for the following set of parameters: $p = 0$, $q = 1$, and $Ng_2 = -0.3$. These differ from the parameters characteristic of experiments [5,14], $p \gg q$, $Ng_2 = -0.03q$, by setting p to zero, and enhancing nonlinearity by an order of magnitude. It should be emphasised that observation times in these experiments are too low for the many-body effects to manifest themselves. Simply extending the "observation" time in simulations allows for the many body effects to be seen, but produces two many oscillations of physical quantities on the relevant time scales. Enhancing the nonlinearity allows one to produce comprehensible graphics, while making no qualitative difference to the condensate evolution. Setting p to zero is of no consequence: in essence this means introducing a reference frame following the Larmor precession.

The number of particles in our simulations was $N = 50$. Importantly, this number is large enough to clearly separate the relaxation and the revival time scales. Indeed, relaxation is exactly that what we expect from a many body treatment, whereas revivals are artifact of the model. At the same time, leaving the atom number relatively low simplifies numerics enormously, making the problem easily tractable on an average desktop computer.

5.3. Evolution of atomic coherence

Fig. 2 shows the evolution of the condensate magnetisation, Eq. (35), calculated both within the many-body model and under the mean-field approximation. With our choice of the initial state and parameters, only the x component of the magnetisation is nonzero. In the mean-field approximation, this component oscillates periodically between values $-N$ and N. *Exact* periodicity follows from the analytical solution [14]. The many body result shows *decaying* oscillations with the same period. Qualitatively, the decay can be understood if considering the simplest generic model of collisional nonlinearity: the Kerr oscillator [23]. The latter is a single-mode quantum oscillator with quartic nonlinearity,

$$\mathscr{H}_{\mathrm{eff}} = \omega_{\mathrm{eff}}\hat{n} + \frac{g_{\mathrm{eff}}}{2}\hat{n}(\hat{n} - 1). \quad (44)$$

Assume the Kerr oscillator is initially in a coherent state with amplitude α. A straightforward calculation of the average position of the oscillator yields,

$$\langle\hat{x}(t)\rangle = \frac{1}{\sqrt{2}}\Re\{\alpha\exp[-\mathrm{i}\omega_{\mathrm{eff}}t + N_{\mathrm{eff}}(\mathrm{e}^{-\mathrm{i}g_{\mathrm{eff}}t} - 1)]\}$$
$$\approx x_{\mathrm{MF}}(t)\mathrm{e}^{-N_{\mathrm{eff}}g_{\mathrm{eff}}^2 t^2/2}, \quad |g_{\mathrm{eff}}t| \ll 1, \quad (45)$$
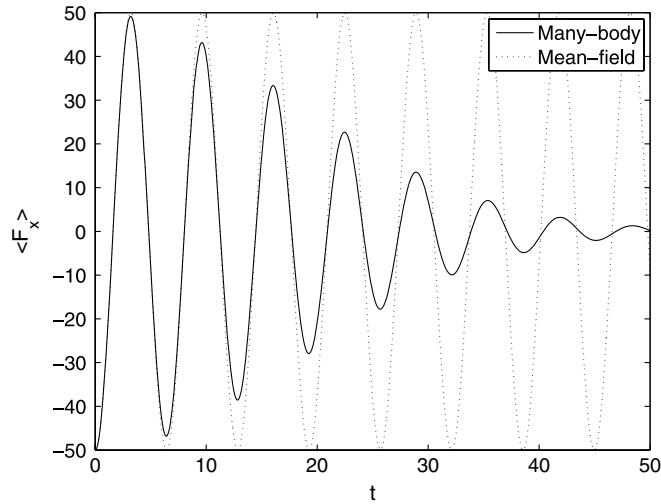
Fig. 2. Evolution of the condensate magnetisation as function of the scaled time. $N = 50$, $p = 0$, $q = 1$, $Ng_2 = -0.3$. Only the x component of the magnetisation is nonzero. In the mean-field approximation, magnetisation oscillates without relaxation.

where $N_{\text{eff}} = |\alpha|^2$ and

$$x_{\text{MF}}(t) = \frac{1}{\sqrt{2}} \Re[\alpha e^{-i(\omega_{\text{eff}} + g_{\text{eff}} N_{\text{eff}})t}], \tag{46}$$

is the mean-field approximation to $\langle \hat{x}(t) \rangle$ which accounts for the frequency shift but not the dephasing. Given the obvious crudeness of the Kerr model, it reproduces the evolution of the magnetisation, Fig. 2, with surprising accuracy. Setting $N_{\text{eff}} g_{\text{eff}}^2 \approx 2Ng_2^2$ results in a good quantitative estimate of the decay time, $\tau_{\text{decay}} \approx (\sqrt{N} g_2)^{-1} \approx 23$. The Gaussian nature of the decay is also evident in Figs. 2 and 3.

Contrary to what could be expected, the system does not evolve towards a spherically symmetric state. A formal indication of this may be seen in Fig. 3. This figure shows
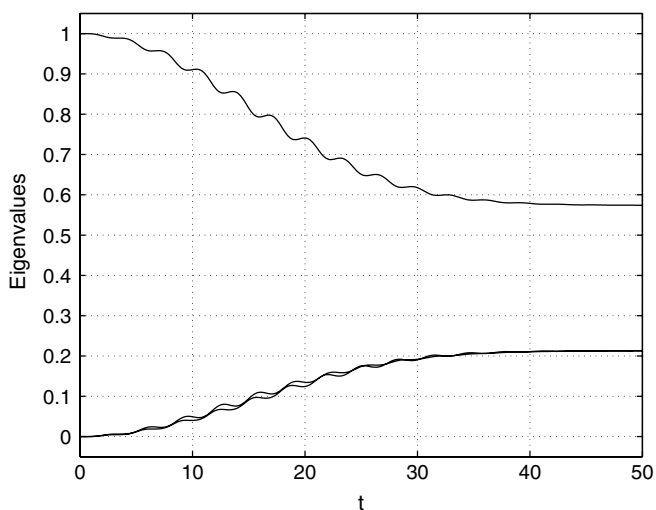

Fig. 3. Scaled eigenvalues of the single-time density matrix. $N = 50$, $p = 0$, $q = 1$, $Ng_2 = -0.3$. In the mean field approximation, one eigenvalue always equals one and the other two eigenvalues are zero.

scaled eigenvalues of the single-body density matrix, cf. Eq. (24). In the mean field approximation, one eigenvalue always equals one and the other two eigenvalues are zero. This holds for the initial state, but for nonzero times we find that all three eigenvalues are nonzero. Most interestingly, they do not evolve towards the value of 1/3 indicative of spherical symmetry. Two of them stabilise at ≈ 0.22, while the third one remains close to ≈ 0.56. Since the magnetisation decays completely, cf. Fig. 2, the persistent asymmetry must be of quadrupole nature.

Being a mathematically rigorous way of characterising alignment, the quadrupole tensor is not the best choice so far as *visualisation* of the results is concerned. A much more convenient way is thinking in terms of the *alignment ellipsoid*. The latter is found by diagonalising the real part of the density matrix, cf. Eq. (31). The eigenvectors of $\Re\rho$ are the alignment axes. The eigenvalues of $\Re\rho$ are positive, their sum equals population, $q_1 + q_2 + q_3 = N$, and differences between them characterise alignment. In particular, three equal eigenvalues, $q_1 = q_2 = q_3 = N/3$, mean the atomic state has no alignment at all. The system of three orthogonal eigenvectors and three positive eigenvalues is naturally visualised as a three-dimensional ellipsoid. If we additionally shift the centre of this alignment ellipsoid by the magnetisation vector, the resulting picture contains all details of the atomic coherence, cf. Fig. 4. An additional simplification is that the smallest axis of the ellipsoid was always found to be collinear with the magnetisation vector. This also holds if $p \neq 0$ when the whole picture is subject to the Larmor precession. Thus the only parameter we need in order to fully specify the orientation of the alignment ellipsoid is the tilt angle; the latter is defined as the angle between the largest axis of the ellipsoid and the quantisation (z) axis. Together with the eigenvalues of $\Re\rho$ [cf. Eq. (31)] and the magnetisation vector, this angle completes characterisation of the atomic coherence.

Visualisation of atomic coherence at different stages of the evolution may be seen in Fig. 4. Evolution of the alignment eigenvalues and of the tilt angle is shown in Fig. 5. At early stages of the evolution, the mean field picture holds with a very good accuracy. In the mean field approximation, the alignment ellipsoid reduces to a flat ellips orthogonal to the magnetisation vector. There are two characteristic moments of the mean-field evolution [cf. Eq. (35) and Fig. 5, top row]. If the magnetisation is maximal, the alignment axis are equal; the alignment ellipsoid becomes a disk (Fig. 5, top-left). If the magnetisation is zero, only one alignment eigenvalue is nonzero; the alignment ellipsoid reduces to a straight line at $\pi/4$ tilt (Fig. 5, top-right). The mean-field evolution of the atomic coherence is in essence periodic oscillations between these characteristic configurations.

On later stages of the evolution the mean field picture breaks down. All three eigenvalues of $\Re\rho$ are nonzero, so that the alignment ellipsoid acquires thickness, becoming an ellipsoid proper (Fig. 4, bottom-left). The tilt oscillations are damped and finally cease (Fig. 5). The final state

of atomic coherence is depicted in Fig. 4, bottom-right. The magnetisation is zero so that the ellipsoid is centered at the centre of coordinates. The larger axis is along z, the other two are equal so that the alignment ellipsoid is axially symmetric. This state of atomic symmetry is impossible to obtain in the mean-field picture.
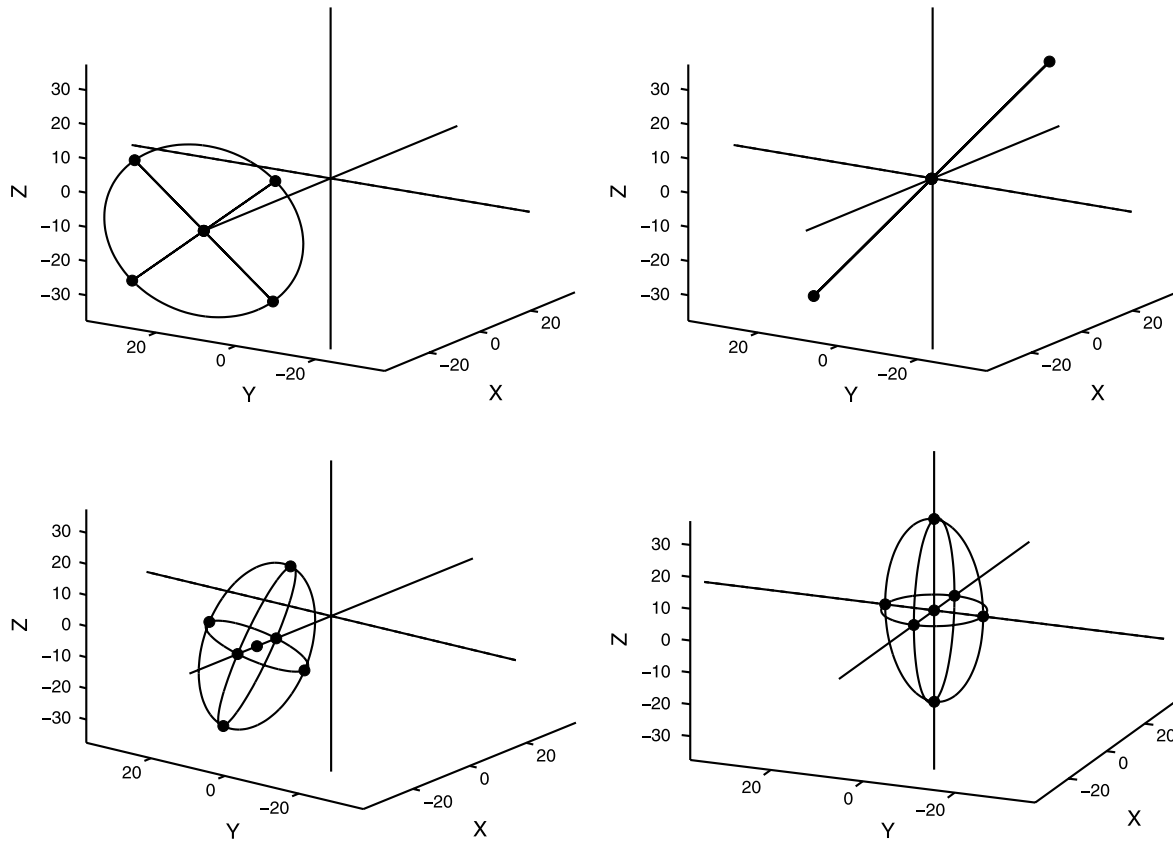

Fig. 4. Visualisation of the time evolution of the condensate coherence. The pictures shows the alignment ellipsoid, the centre of which is shifted by the magnetisation vector. One of the alignment axis is always collinear with the magnetisation vector, so that the only parameter specifying the ellipsoid's orientation is the tilt angle. In the mean-field approximation, the ellipsoid reduces to a flat ellips orthogonal to the magnetisation vector. Top row: initial stages of the evolution at which the mean-field picture is valid. Left: the initial state of the condensate coherence. The alignment ellipsoid is reduced to a disc. Right: the condensate coherence at zero magnetisation. The alignment ellipsoid is reduced to a straght line in the yz plane with $\pi/4$ tilt. Bottom row: later stages of the evolution at which the mean-field picture fails. Left: a typical picture of coherence at intermediate stages of the evolution. Right: the final state of condensate coherence. The magnetisation and tilt are zero, and the ellipsoid is axially symmetric in respect of the quantisation axis.
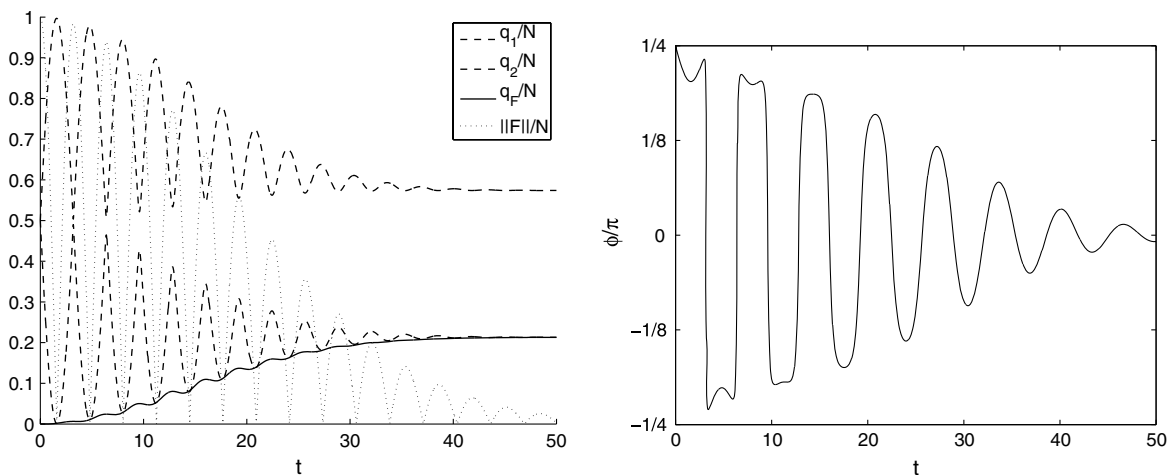

Fig. 5. Evolution of the quadrupole. $N = 50$, $p = 0$, $q = 1$, $Ng_2 = -0.3$. Left: the alignment eigenvalues, right: the tilt angle. The smallest eigenvalue corresponding to the alignment axis along the magnetisation is shown as solid line, the other two – as dashed lines. The modulus of magnetisation (dotted line) helps to visually synchronise this picture with Fig. 2. In the mean field approximation, the smallest eigenvalue is exactly zero while the other two eigenvalues and the tilt oscillate periodically without relaxation.

Thus in the course of the evolution atomic coherence undergoes a complete change of symmetry. Initially, the system is prepared in an axially symmetric state in respect of the x axis. At intermediate stages of the evolution, all symmetries are broken. Finally, the system again tends towards an axial symmetry. Not unexpectedly, the final symmetry coincides with the dynamical symmetry, with the symmetry axis parallel to the magnetic field.

6. Conclusion

We have modelled the quantum many-body dynamics of a spin-1 condensate numerically within a single mode approximation, using the representation of irreducible tensor operators so as to conveniently visualise the condensate evolution. Comparing results of the numerical simulation to those obtained within the mean field approximation shows a number of characteristic features of the many-body evolution which are impossible to obtain under the mean field approximation. In particular, the final state of the condensate coherence is of a characteristic quadrupole nature, axially symmetric in respect of the quantisation axes, whereas this kind of atomic coherence is impossible in principle in the mean field approximation. Experimentally observing this state of atomic coherence would be a distinct signature of spin-mixing collisions without the mean-field approximation.

Acknowledgements

Appendix A. Implementation of many-body operators in the fock space

To be specific, consider how mode annihilation operators, $\hat{a}_k$, are implemented in a high-level numerical package. Such packages handle sparse rectangular matrices very effectively, so the first step is to replace a triple index, $\{N_1, N_0, N_{-1}\}$, characterising a basis state in the Fock space, by a linear index. A helpful trick is to start from introducing an extended index, $n = 1 + N_1 + (N+1)N_0$, where $0 \leqslant N_1, N_0 \leqslant N$. The third index, N_{-1}, is found from $N_1 + N_0 + N_{-1} = N$. Each value of the extended index, $1 \leqslant n \leqslant (N+1)^2$, thus corresponds to a unique triple,

$$N_1(n) = (n-1)\bmod(N+1),$$
$$N_0(n) = \frac{n-1-N_1(n)}{N+1}, \qquad (A.1)$$
$$N_{-1}(n) = N - N_1(n) - N_0(n).$$

This includes nonphysical entries with $N_{-1}(n) < 0$ which are to be filtered out later. The advantage of using the extended indexing is that, as a rule, many-body operators

written in the extended index are simple banded matrices. For example, if $k = 1, 0$,

$$\langle n' | \hat{a}_k | n \rangle = \delta_{n', n-\Delta_k} \sqrt{N_k(n)}, \quad \Delta_k = (N+1)^{1-k}. \qquad (A.2)$$

That is, in the extended index, $\hat{a}_1$ and $\hat{a}_0$ are sparse matrices with a single nonzero side diagonal. Generating such matrices numerically is straightforward; $\hat{a}_{-1}$ which is not found in such simple way can then be obtained by a suitable permutation of rows and columns of $\hat{a}_1$ (say). In the matrices generated using Eq. (A.2) one should retain only columns for which $N_{-1}(n) \geqslant 0$ and rows for which $0 \leqslant N_{-1}(n') \leqslant N - 1$ and $N_1(n')$, $N_0(n') \leqslant N - 1$. (Recall that $\hat{a}_k$ acts from the subspace of N atoms into the subspace of $N - 1$ atoms.) This is equivalent to building a "physical" linear index, changing N_1 first, and N_0 – second, while watching for the condition $N_1 + N_0 \leqslant N$; however the property of having a single nonzero side diagonal does not hold for the physical indexing. Generalisation to higher-order spin values is straightforward.

There is a further subtlety in how products of field operators are implemented numerically. An unwanted by-product of introducing field operators is a formal non-conservation of the particle number. We wish to restrict ourselves to a subspace of given N and introduce annihilation operators as acting from this subspace into the subspace of $N - 1$ atoms. Then, only bilinear normally ordered operator products, $\hat{a}_k^\dagger \hat{a}_l$, are immediately defined for numerical purposes. Viewed literally, quartic normally ordered operators products [cf. the first line of Eq. (9)] imply knowledge of the field operators acting from the subspace of $N - 1$ atoms into the subspace of $N - 2$ atoms and hence cannot be implemented under this restriction. The solution to this problem is obvious: use commutation relations. So, with $\mathscr{I}_N$ being the unit matrix in the subspace of N atoms,

$$\hat{a}_l \hat{a}_k^\dagger = \hat{a}_k^\dagger \hat{a}_l, \quad k \neq l,$$
$$\hat{a}_k \hat{a}_k^\dagger = \hat{a}_k^\dagger \hat{a}_k + \mathscr{I}_N, \qquad (A.3)$$
$$\hat{a}_k^\dagger \hat{a}_k^\dagger \hat{a}_k \hat{a}_k = (\hat{a}_k^\dagger \hat{a}_k)^2 - \hat{a}_k^\dagger \hat{a}_k,$$

etc. [cf. also the second line of Eq. (9)]. Eq. (A.3) hold in the complete Fock space, but only their right-hand sides make numerical sense under the above restriction.

References

[1] B.W. Shore, The Theory of Coherent Atomic Excitation, vols. 1 and 2, Wiley, New York, 1989.
[2] C.J. Pethick, H. Smith, Bose–Einstein Condensation in Dilute Gases, Cambridge University Press, Cambridge, 2002.
[3] D.M. Stamper-Kurn et al., Phys. Rev. Lett. 80 (1998) 2027.
[4] M.D. Barrett, J.A. Sauer, M.S. Chapman, Phys. Rev. Lett. 87 (1998) 010404.
[5] H. Schmaljohann et al., Appl. Phys. B 79 (2004) 1001.
[6] T.-L. Ho, Phys. Rev. Lett. 81 (1998) 742.
[7] T. Ohmi, K. Machida, J. Phys. Soc. Jpn. 67 (1998) 822.
[8] C.K. Law, H. Pu, N.P. Bigelow, Phys. Rev. Lett. 81 (1998) 5257.
[9] H.-J. Miesner et al., Phys. Rev. Lett. 82 (1999) 2228;
D.M. Stamper-Kurn et al., Phys. Rev. Lett. 83 (1998) 661.

[10] A. Omont, Progr. Quant. Electron. 5 (1977) 69.
[11] D.A. Varshalovich, A.N. Moskalev, V.K. Khersonskii, Quantum Theory of Angular Momentum, World Scientific, Singapore, 1988.
[12] M. Koashi, M. Ueda, Phys. Rev. Lett. 84 (2000) 1066.
[13] M.-S. Chang et al., e-print cond-mat/0509341.
[14] J. Kronjäger et al., Phys. Rev. A 72 (2005) 063619.
[15] A. Griesmaier et al., Phys. Rev. Lett. 94 (2005) 160401.
[16] L. Santos, T. Pfau, e-print cond-mat/0510634.
[17] Y. Kawaguchi, H. Saito, M. Ueda, Phys. Rev. Lett. 96 (2006) 080405.
[18] W. Zhang et al., Phys. Rev. Lett. 95 (2005) 180403.
[19] W. Zhang et al., Phys. Rev. A 72 (2005) 013602.
[20] J. Vanier, C. Audoin, The Quantum Physics of Atomic Frequency Standards, Hilger, Philadelphia, 1988.
[21] M.-S. Chang et al., Phys. Rev. Lett. 92 (2004) 140403.
[22] M. Steel et al., Phys. Rev. A 58 (1998) 4824.
[23] A. Imamoglu, M. Lewenstein, L. You, Phys. Rev. Lett. 78 (1997) 2511.